J Comput Aided Mol Des (2013) 27:605–614
DOI 10.1007/s10822-013-9665-3

In silico molecular docking analysis of the human Argonaute 2 PAZ domain reveals insights into RNA interference

Mahmoud Kandeel · Yukio Kitade

Received: 28 April 2013 / Accepted: 5 July 2013 / Published online: 23 July 2013

Abstract RNA interference (RNAi) is a critical cellular pathway activated by double stranded RNA and regulates the gene expression of target mRNA. During RNAi, the 3′ end of siRNA binds with the PAZ domain, followed by release and rebinding in a cyclic manner, which deemed essential for proper gene silencing. Recently, we provided the forces underlying the recognition of small interfering RNA by PAZ in a computational study based on the structure of *Drosophila* Argonaute 2 (Ago2) PAZ domain. We have now reanalyzed these data within the view of the new available structures from human Argonauts. While the parameters of weak binding are correlated with higher (RNAi) in the *Drosophila* model, a different profile is predicted with the human Ago2 PAZ domain. On the basis of the human Ago2 PAZ models, the indicators of stronger binding as the total binding energy and the free energy were associated with better RNAi efficacy. This discrepancy might be attributable to differences in the binding site topology and the difference in the conformation of the bound nucleotides.

Keywords RNA interference · Gene silencing · Argonaute proteins · PAZ domain · Computational analysis · Molecular docking

M. Kandeel (✉)
Department of Pharmacology, Faculty of Veterinary Medicine, Kafrelshiekh University, Kafrelshiekh 33516, Egypt
e-mail: mahmoud.kandeal@vet.kfs.edu.eg

M. Kandeel · Y. Kitade
United Graduate School of Drug Discovery and Medical Information Sciences, Gifu University, Gifu, Japan

Y. Kitade (✉)
Department of Biomolecular Science, Faculty of Engineering, Gifu University, Yanagido 1-1, Gifu 501-1193, Japan
e-mail: ykkitade@gifu-u.ac.jp

Introduction

Small RNAs are 20–30 nucleotides in length and have an indispensable role in the regulation of various cellular processes [1]. They can target both chromatin and transcripts, thus it keeps both genome and transcriptome under strict surveillance [2]. The relationship between small RNAs and their molecular targets has been studied extensively [3–5]. Within the extensive study of RNA interference, special attention has been directed to its use in anticancer therapy [6–8], cell proliferation and apoptosis [9], antiviral therapy [10], overcoming drug resistance [11], and as a therapeutic approach in treating asthma [12, 13], rheumatoid arthritis [14, 15], as an adjunct therapy in diabetes [16], and other diseases [17, 18]. The major integrators of this process include a small RNA (either produced intracellularly or transfected into the cells) and a set of cellular macromolecular proteins to form RNA-induced silencing complex (RISC). The net effect of the process is regulation of the target gene expression by destroying its transcribed mRNA. Recently, we mentioned that during the RNAse activity of RISC-RNA complex, the 3′ end of siRNA toggles between binding and release from the binding cavity of PAZ domain [19]. These changes were found to be essential for proper functioning of mRNA cleavage. In comparison with 12-nucleotide target RNA, the binding of a 15-nucleotide target RNA is accompanied by pivotal rotation of PAZ domain [20]. Recently, it was reported that PAZ domain is essential in RNAi process. PAZ-disrupted Ago mutants were unable to unwind or eject the passenger strand of miRNA-like mismatch-containing duplexes [21].

Several studies have focused on the functional aspects of the attaching 3′ end of siRNA with its binding pocket of Argonautes PAZ domain [22–26]. Furthermore, using a computational approach, we recently tested the hypothesis that the binding strength of the 3′ end of siRNA can affect the

overall RNAi process. During our previous study, we used a model based on the structure of *Drosophila* PAZ domain bound with siRNA. Recently, the structure of full length human Ago2 including its four classical domains (PAZ, MID, N-terminal and PIWI domains) was resolved [27, 28]. Despite the high homology between the human and *Drosophila* PAZ domains, there are significant changes in the contour of the binding pockets as well as in the orientation and conformation of the bound nucleotides (Figs. 1, 2). To address whether there is a difference between the two models, we reanalyzed the correlation of the in vivo RNAi efficacy data by using the new human Ago2 PAZ domain structures and compared these with our previously analyzed data [19]. Despite the large amount of research dedicated to RNAi, it is not well understood whether compounds with stronger or weaker binding with the human Ago2 PAZ domain could enhance or hinder the whole RNAi process. This study was performed to explore the effect of weaker or stronger binding of siRNA on overall RNAi effects. The stronger binding with the PAZ domain might interfere with the previously mentioned siRNA binding-release cycle, thereby affecting the whole RNAi process. For this purpose, we reanalyzed the experimentally determined gene silencing of modified siRNAs (Fig. 3) produced previously by our lab and then correlated these results with computational and modeling tools.

Methods

Molecular docking studies

Preparation of compounds

Several siRNA 3′ overhang modifications were developed in our lab [23, 29–35]. The structure of these compounds together with their in vivo efficacy were retrieved and subjected to further investigations including docking studies and computational tools. Compounds conformation and orientation relative to the binding site was computed by using a generic evolutionary method provided by i-GEMDOC [36, 37]. Cleaning and optimization of compounds conformation was carried out by ChemSketch

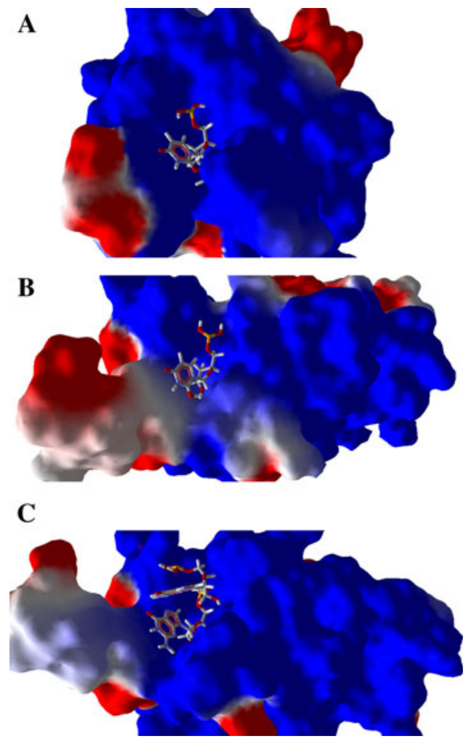

Fig. 2 Surface representation of human and *Drosophila* Ago2 PAZ domain. The *Drosophila* Ago2 PAZ domain bound with 2′-*O*-methyl uridine (*upper*). The human Ago2 PAZ domain is bound with uridine (*middle*) or guanosine (*lower*)

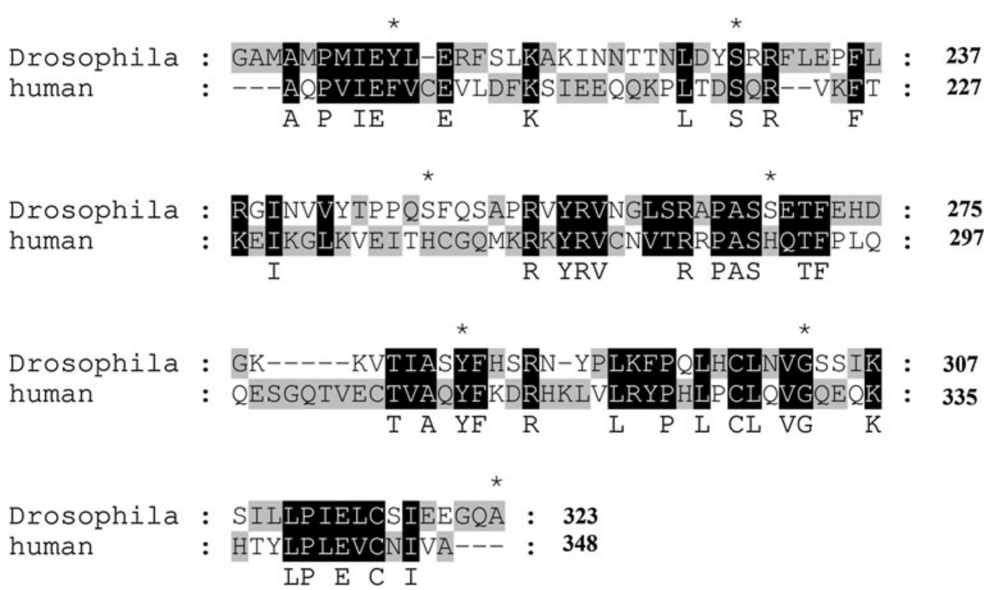

Fig. 1 Alignment of human and *Drosophila* Ago2 PAZ domain. The figure is generated by GeneDoc software

compound	structure	RL/FL	Compound	structure	RL/FL	compound	structure	RL/FL
t	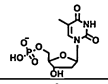	0.48	u1	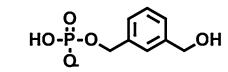	0.5	u12	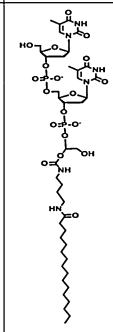	0.6
tt	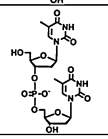	0.29	u2	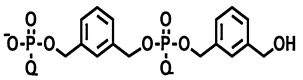	0.4			
ttt	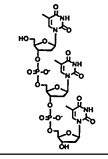	0.28	u3	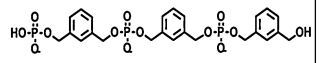	0.4			
u4	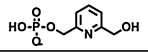	0.42	u5	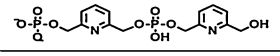	0.3	u13	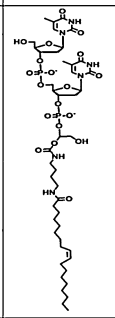	0.7
u7	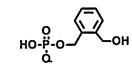	0.3	u6	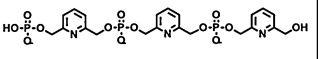	0.3			
u8	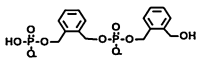	0.32	u9	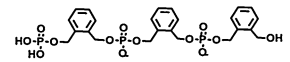	0.4			
u10bb	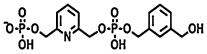	0.2	u11btbt	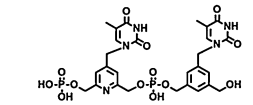	0.4			
u15BpBp	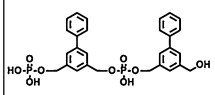	0.58	u16BnBn	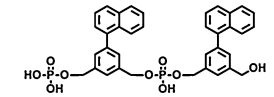	0.7	u14	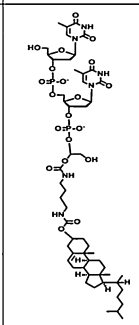	1.1
u17BhBh	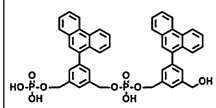	0.78	u18	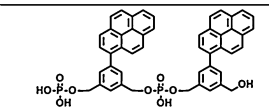	1.1			
u19BBn	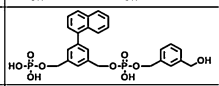	0.74	u20BB	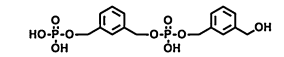	0.3			
u21RHRH	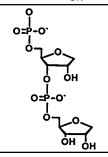	0.19	Utd1	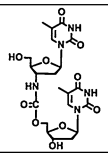	0	UTD2	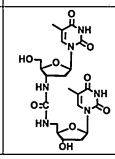	0.3

Fig. 3 The compounds used in this study

12.01 software (ACDlabs, Canada) and Openbabel software version 3.2.1.

Preparation of protein

The crystal structure of human Ago2 was used for docking studies (PDB ID 4EI1 and 4F3T). In these structures, the PAZ domain was identified and isolated by using Discovery Studio software. The binding cavity was isolated by using Deep View Swiss PDB viewer software. The bound nucleotide was picked as a guide to isolate the neighboring residues within the range of 12 Å.

Docking Docking studies were performed by using iGEMDOCK as well as by using the automated functions available at the docking server (http://www.docking-server.com/). In order to get accurate docking, stable (slow) docking was used as a default setting. Blind docking runs and repeats of runs with the same compounds were carried out to avoid false positive or false negative results.

In iGEMDOCK, the parameters of docking run were set as population size (N = 300), generations (80), number of solutions (10). The best pose was selected based on the best conformation that allows the lowest free energy of binding.

The docking server [38] is based on MMFF94 force field for energy minimization of ligand molecules. Gasteiger partial charges were added to the ligand atoms. Non-polar hydrogen atoms were merged, and rotatable bonds were defined. Essential hydrogen atoms, Kollman united atom type charges, and solvation parameters were added with the

aid of AutoDock tools. Affinity (grid) maps of 20 × 20 × 20 Å grid points and 0.375 Å spacing were generated using the Autogrid program. AutoDock parameter set-and distance-dependent dielectric functions were used in the calculation of the van der Waals and the electrostatic terms, respectively. Docking simulations were performed using the Lamarckian genetic algorithm (LGA). Initial position, orientation, and torsions of the ligand molecules were set randomly. Each docking experiment was derived from 10 different runs that were set to terminate after a maximum of 2,50,000 energy evaluations. The population size was set to 150. During the search, a translational step of 0.2 Å, and quaternion and torsion steps of five were applied. The total intermolecular energy is the sum of electrostatic energy, hydrogen bonding, van der Waals and desolvation energy. The free energy is calculated as the following equation [39]:

Table 1 The docking results by using iGEMDOCK

Compound	Total energy	VDW	HBond	Elec	RL/FL
t	−88.5214	−52.4624	−36.059	0	0.48
tt	−125.159	−83.1183	−41.3621	−0.679094	0.29
ttt	−156.086	−103.128	−42.4703	−10.4877	0.28
U1	−67.1552	−54.2964	−12.8588	0	0.48
U2	−120.28	−74.5983	−43.1051	−2.57623	0.37
U3	−130.737	−93.0803	−30.354	−7.30262	0.4
U4	−77.5497	−40.0158	−33.8087	−3.72522	0.42
U5	−115.506	−62.8486	−49.27	−3.38779	0.32
U6	−131.705	−105.981	−20.1138	−5.60976	0.34
U7	−69.0669	−54.3169	−14.75	0	0.3
U8	−111.84	−66.2657	−35.2723	−10.3016	0.32
U9	−135.278	−93.1873	−31.4594	−10.6313	0.36
U10bbn	−114.912	−73.059	−34.2833	−7.56965	0.2
U11btbt	−164.876	−125.704	−32.242	−6.92963	0.37
U12	−139.989	−90.9922	−41.7795	−7.21683	0.6
U13	−144.218	−115.042	−26.0183	−3.15711	0.65
U14	−159.588	−135.32	−22.2558	−2.01212	1.1
U15BbBb	−148.842	−109.317	−31.1999	−8.32479	0.58
U16BnBn	−135.726	−95.56	−31.2485	−8.91747	0.7
U17BhBh	−151.7	−102.121	−40.2848	−9.29479	0.78
U18ByBy	−139.607	−117.998	−16.51	−5.09863	1.05
u19bBBn	−111.867	−89.8929	−21.9741	0	0.74
u20BB	−107.487	−64.3429	−35.4222	−7.72172	0.26
Utd1	−110.236	−55.1383	−49.862	−5.23609	0.3
Utd2	−120.955	−95.5384	−25.4163	0	0.28
U21RHRH	−126.048	−84.5088	−41.5395	0	0.19

The used template is derived from PDB ID 4F3T (bound with uridine). The output data included total energy (kcal/mol), van der Waals interactions (VDW, kcal/mol), hydrogen bonding (HBond, kcal/mol), electrostatic interactions and (elec, kcal/mol). RL/FL indicates *Renilla* luciferace expression normalized by firefly luciferase data

$$\triangle G = \triangle G\text{vdw} + \triangle G\text{hbond} + \triangle G\text{elec} + \triangle G\text{conform} + \triangle G\text{tor} + \triangle G\text{sol} \quad (1)$$

Statistical analysis

The data set obtained from the computational tools was correlated with RANi efficacy. Pearson's correlation coefficient and the significance of correlation were estimated by STATA statistical package (version 12.1). The results are provided in Tables 5, 6, 7 and 8.

Other modeling methods

Protein surfaces were generated by Molegro viewer. The sequences of human and *Drosophila* Ago2 PAZ domain were retrieved from the protein sequences database (http://www.ncbi.nlm.nih.gov/protein). The sequences are aligned by using ClustalW (http://www.ebi.ac.uk/Tools/msa/clustalw2/). The identity and similarity of sequences were calculated by EMBOSS Matcher server (http://www.ebi.ac.uk/Tools/psa/emboss_matcher/).

Results and discussion

The alignment of human and *Drosophila* Ago2 PAZ domain sequences (Fig. 1) revealed high homology (about 42 % identity and 60 % similarity, calculated by EMBOSS matcher software). The surface representation of PAZ domains and the conformation of the nucleotides at the 3′ end of RNA is provided in Fig. 2. While there is high similarity between the human and *Drosophila* Ago2 PAZ domains, there was a noticeable difference in the conformation of the bound substrates (Fig. 2).

The detailed output parameters of docking runs are given in Tables 1, 2, 3 and 4. Two different docking programs were used (iGEMDOCK and the docking server). Furthermore, two available sources of human Ago2 PAZ domain, 4EI1 bound with guanosine and 4F3T bound with uridine. The last column of Tables 1, 2, 3 and 4 indicates the ability of siRNAs to suppress gene expression, as determined by a dual-luciferase reporter assay with *Renilla* and firefly luciferase genes as reporter genes [23, 31–35]. All measured data are at 1 nM of siRNA concentration. The signal of *Renilla* luciferase was normalized to that of firefly luciferase. The lower RL/FL indicates lower gene expression and potent RNAi activity. In contrast, higher RL/FL indicates lower potency of siRNA.

Correlation of the total and free energy of binding and RNAi

The total and free energy of binding are indicating the sum of all forces during protein-siRNA recognition. Therefore,

it is likely to be the most sensitive parameter that implies the strength of binding. There was a positive correlation between the total (Tables 5, 6) and free energy (Tables 7, 8) with RNAi. The positive correlation of the total energy and RNAi showed statistically significant values ($R = 0.804$, Table 5). Similarly, the estimated free energy showed significant statistical correlation with the detected RNAi ($R = 0.421$, Table 8). That means the lower values of energy (stronger binding) is associated with lower values of RL/FL (i.e. better RNAi efficacy).

In our previous report, we used the available structure of *Drosophila* Ago2 PAZ domain, in which we reported a weak binding affinity is favourable for RNAi. In parallel, the binding affinity of *Drosophila* PAZ domain was found to be within weak-to-moderate affinity range [40]. A similar finding was reported after titration of *Drosophila* Ago2 PAZ domain with siRNAs [41]. Therefore, weak-moderate binding affinity was a regular finding with *Drosophila* PAZ domain. In this context, approximately 2 decades ago, early studies on Ago2 PAZ domain were from *Drosophila* or microorganisms. These studies showed low binding affinity with siRNAs. Recently, the structure of human Ago2 is resolved; however, the binding affinity and specificity of the human Ago2 PAZ domain have yet to be characterized.

Table 2 The docking results by using iGEMDOCK

Compound	Total energy	VDW	HBond	Elec	RL/FL
t	−107.245	−68.0161	−32.0929	−7.13582	0.48
tt	−129.694	−92.0848	−33.4801	−4.12929	0.29
ttt	−157.517	−120.887	−33.4754	−3.15485	0.28
U1	−88.0742	−59.1154	−21.3995	−7.5593	0.48
U2	−113.125	−70.5217	−31.8768	−10.7263	0.37
U3	−154.82	−99.8483	−44.5938	−10.3779	0.4
U4	−156.126	−108.295	−38.1081	−9.72321	0.42
U5	−119.681	−83.4606	−28.8941	−7.32599	0.32
U6	−153.042	−106.248	−40.7353	−6.05843	0.34
U7	−130.516	−81.8064	−41.9987	−6.71066	0.3
U8	−169.387	−131.004	−34.6812	− 3.70184	0.32
U9	−136.354	−100.526	−28.8424	−6.98594	0.36
U10bbn	−142.518	−108.478	−26.8525	−7.18727	0.2
U11btbt	−152.158	−101.618	−39.3757	−11.1642	0.37
U12	−133.462	−120.507	−12.9553	0	0.6
U13	−145.732	−90.453	−45.5171	−9.76164	0.65
U14	−120.475	−107.475	−13	0	1.1
U15BbBb	−120.882	−68.5132	−41.0971	−11.2717	0.58
U16BnBn	−115.689	−77.7097	−29.5969	−8.38221	0.7
U17BhBh	−120.594	−68.4811	−43.6698	−8.44278	0.78
U18ByBy	−135.431	−106.55	−23.27	−5.61073	1.05
u19bBBn	−90.584	−56.5704	−25.9784	−8.03521	0.74
u20BB	−126.881	−78.7952	−37.8119	−10.2735	0.26
Utd1	−134.065	−95.9291	−30.0877	−8.04841	0.3
Utd2	−85.0552	−59.953	−18.1163	−6.98594	0.28
U21RHRH	−116.377	−64.9436	−37.5522	−13.8808	0.19

The used template is derived from PDB ID 4EI1 (bound with guanosine). The output data included total energy (kcal/mol), van der Waals interactions (VDW, kcal/mol), hydrogen bonding (HBond, kcal/mol), and electrostatic interactions (elec, kcal/mol). RL/FL indicates *Renilla* luciferace expression normalized by firefly luciferase data

The comparison between the estimated free energy from all used models is shown in Fig. 4. Within all the used models, hGG (human PAZ domain bound with guanosine) showed the lowest free energy estimate as well as the lowest total energy (Fig. 5). Interestingly, the range of compounds which showed higher total energy with hGG (compounds U14-u19BBn) was associated with the higher RL/FL ratio (Tables 1, 2).

The other binding parameters

Within the analyzed models, a remarkable variability was detected with hydrogen bonding and electrostatic energy (Fig. 6). Weak correlation with RF/LF is associated with hydrogen bonding (Tables 5, 6). In contrast, moderate-strong correlation with RF/LF ratio was predicted with van der Waals interaction (Tables 5, 6), as well as electrostatic interactions (Tables 7, 8). This supports the above prediction that stronger binding is more favourable for association of siRNAs with human PAZ domain. The lower values of van der Waals and electrostatic energy are almost associated with stronger binding.

Comparison of the different models used in this study is represented as 100 % area plot in Fig. 6. The values of hGG (human PAZ domain bound with guanosine) are showing the lowest van der Waals values. In contrast, a noticeable difference in the predicted values with hU model (PAZ domain bound with uridine). The discrepancy between the used human PAZ domains models in Figs. 4, 5, and 6 may arise from the difference in the bound ligand (guanosine and uridine). Such difference may contribute to the subtle changes in the estimated docking parameters.

Analysis of the binding forces indicates that hydrogen bonding and van der Waals interaction are the major contributor to the binding affinity, followed by the electrostatic energy as a minor contributor. Realizing that phosphate groups of natural nucleotides are the main source of electrostatic interactions with the cavity of the PAZ domain, modifying phosphate groups will not lead to major changes in compounds binding. However, this could come on the expense of hydrogen bonding. It was reported that the first phosphate group is associated with an important hydrogen bonding with the backbone of PAZ domain [27]. Modifications including the phosphate group might improve the resistance of siRNAs against nucleases. However, the proposed change should not be at the expense of the contacts of the phosphate group with PAZ domain.

Table 3 The docking results by using the docking server

Compound	Estimated free energy	Inhibition constant Ki	vDw + Hbond + desolvation energy	Electrostatic energy	Total intermolecular energy	Interaction surface	RL/FL
t	−5.54	87.09	−6.29	−0.07	−6.35	539.81	0.48
tt	−4.65	388.44	−6.6	−0.38	−7.04	736.18	0.29
ttt	−13.51	ND	−5.67	−0.07	−6.37	963.1	0.28
U1	−4.6	426.55	−6.05	−0.01	−6.06	488.33	0.48
U2	−5.88	49.1	−8.24	−0.51	−8.75	690.67	0.37
U3	−3.69	1,960	−7.56	−1	−8.55	846.3	0.4
U4	−4.68	370.96	−5.6	−0.05	−5.65	453.94	0.42
U5	−4.78	315.12	−6.38	−0.6	−6.98	567.21	0.32
U6	−3.65	2,110	−7.83	−1.15	−8.98	786	0.34
U7	−5.08	188.38	−5.46	−0.04	−5.5	408	0.3
U8	−4.98	223.44	−7.49	−0.32	−7.82	685.54	0.32
U9	−3.43	3,040	−7.51	−0.93	−8.45	944.16	0.36
U10bbn	−5.32	127	−7.54	−0.47	−8.01	630.12	0.2
U11btbt	−4.22	800.48	−8.1	−0.33	−8.42	864.9	0.37
U12	174.9	nd	79.39	−1.94	77.46	1,188	0.6
U13	1.07	nd	−4.96	+0.01	−4.95	848.9	0.65
U14	+2.2	nd	−6.25	−0.01	−6.25	868.92	1.1
U15BbBb	−4.61	419.79	−8.31	−0.35	−8.67	863.46	0.58
U16BnBn	−4.61	419.79	−8.3	−0.35	−8.67	863.46	0.7
U17BhBh	−3.24	4,230	−6.81	−0.41	−7.21	904.45	0.78
U18ByBy	−4.1	4,280	−10.41	−0.36	−12.05	891.6	1.05
u19bBBn	−5.52	89.93	−7.87	−0.43	−8.3	741.39	0.74
u20BB	−4.87	315.28	−6.75	−0.52	−7.27	617.4	0.26
Utd1	−4.63	405.33	−6.63	+0.04	−6.59	767.94	0.3
Utd2	−4.39	602.2	−6.96	−0.03	−6.99	727.3	0.28
U21RHRH	−4.21	822.92	−5.72	−0.4	−6.13	638.85	0.19

The used template is derived from PDB ID 4F3T (bound with uridine). The output data included free energy (kcal/mol), inhibition constant (μM), van der Waals interactions, hydrogen bonding and desolvation energy (kcal/mol), electrostatic energy (kcal/mol) and interaction surface. RL/FL indicates *Renilla* luciferase expression normalized by firefly luciferase data

Total interaction surface

A small interaction surface remains a favourable parameter for higher RNAi. The docking results revealed a statistically significant correlation between the size of the interaction surface and RNAi (Tables 7, 8).

The biological relevance of this study

During the RNAse activity of RISC–RNA complex, the 3′ end of siRNA toggles between binding and release from the binding cavity of PAZ domain. These changes were found to be essential for proper functioning of mRNA cleavage. In free state of Ago-siRNA complex, the 3′ of siRNA is bound to the hydrophobic cavity of PAZ domain [20, 42]. For propagation of base pairing with target sequence, the 3′ of siRNA has to be dislodged from its binding pocket of PAZ domain. This is especially important for accommodating different lengths of the bound siRNA and different lengths of base-pairings with target sequences. Thus, there is an inherent confusion about the nature of binding interactions of 3′ terminal of siRNA with PAZ domain. Stable complexes of 3′ terminal of siRNA with PAZ domain are required during binding of dsRNA, during unwinding and release of the passenger strand. This is also important for guiding the RISC complex to bind with the target mRNA. In contrast, the release of 3′ terminal of siRNA from PAZ domain is important for target cleavage. In this study, we tried to conclude the forces of 3′ recognition by PAZ domain. Recently, it was reported that PAZ domain is essential in RNAi process. PAZ-disrupted Ago mutants were unable to unwind or eject the passenger strand of miRNA-like mismatch-containing duplexes [43]. Interestingly, it was reported that PAZ domain undergoes significant molecular dynamics upon binding with target RNAs of different lengths. In

Table 4 The docking results by using the docking server

Compound	Estimated free energy	Inhibition constant Ki	vDw + Hbond + desolvation energy	Electrostatic energy	Total intermolecular energy	Interaction surface	RL/FL
t	−5.89	47.87	−6.65	−0.09	−6.74	555.75	0.48
tt	−7.38	3.89	−8.26	−0.8	−9.06	780.24	0.29
ttt	−7.39	ND	−4.67	−1.5	−6.17	1204.4	0.28
U1	−5.01	212.78	−6.37	−0.06	−6.43	493.4	0.48
U2	−5.98	41.25	−7.88	−0.93	−8.81	801.4	0.37
U3	−5.41	109	−6.49	−2.5	−8.99	846.3	0.4
U4	−5.22	150.15	−5.54	−0.04	−5.58	442.32	0.42
U5	−6.62	13.97	−7.62	−1.03	−8.65	608.24	0.32
U6	−5.37	115.93	−7.47	−1.54	−9.01	735.75	0.34
U7	−5.24	145.21	−6.03	+0.02	−6	444.7	0.3
U8	−6.6	14.63	−9.09	−0.48	−9.57	700.94	0.32
U9	−5.83	52.93	−8.28	−1.29	−9.57	836.68	0.36
U10bbn	−6.23	27.07	−7.32	−1.09	−8.42	654.89	0.2
U11btbt	−4.22	800.48	−8.1	−0.33	−8.42	864.9	0.37
U12	−5.38	113.86	−7.45	−0.74	−8.19	890.66	0.6
U13	−0.52	4,16,000	−8.39	+0.06	−8.33	880.36	0.65
U14	−2.68	10,890	−6.35	−0.06	−6.42	1004.55	1.1
U15BbBb	−8.85	325.38	−10.23	−0.78	−11	953	0.58
U16BnBn	−7.98	1.42	−9.68	−0.48	−10.17	846.46	0.7
U17BhBh	−7.22	5.09	−10.11	−0.79	−10.9	954	0.78
U18ByBy	−5.84	52.09	−9.34	−0.49	−9.83	1133.9	1.05
u19bBBn	−6.61	14.3	−9.24	−0.65	−9.9	811.57	0.74
u20BB	−6.45	18.6	−7.32	−1.14	−8.46	678.6	0.26
Utd1	−6.58	14.95	−7.4	+0.02	−7.38	750.55	0.3
Utd2	−6.37	21.5	−6.24	0.0	−6.24	802.67	0.28
U21RHRH	−6.07	35.55	−7.94	−0.63	−8.58	649.56	0.19

The used template is derived from PDB ID 4EI1 (bound with guanosine). The output data included free energy (kcal/mol), inhibition constant (μM),van der Waals interactions, hydrogen bonding and desolvation energy (kcal/mol), electrostatic energy (kcal/mol) and interaction surface. RL/FL indicates *Renilla* luciferase expression normalized by firefly luciferase data

Table 5 Correlation analysis for RNAi activity and the measured parameters produced by iGEMDOCK

	Total energy	VDW	HBond	Elec	RL/FL
Total energy	1.00				
VDW	0.924*	1.00			
HBond energy	0.0161	−0.29	1.00		
Elec	0.4237*	−0.304	0.2542	1.00	
RL/FL	0.804*	0.769*	−0.0564	0.317	1.00

The used template is derived from PDB ID 4EI1 (bound with guanosine). Pearson's correlation coefficient is calculated by STATA. Data showing significant correlation at 0.05 level are marked by asterisk

Table 6 Correlation analysis for RNAi activity and the measured parameters produced by iGEMDOCK

	Total energy	VDW	HBond	Elec	RL/FL
Total energy	1.00				
VDW	0.839*	1.00			
HBond energy	0.4366*	−0.026	1.00		
Elec	−0.159	−0.495*	0.504*	1.00	
RL/FL	0.204	0.151	0.041	0.674*	1.00

The used template is derived from PDB ID 4F3T (bound with uridine). Pearson's correlation coefficient is calculated by STATA. Data showing significant correlation at 0.05 level are marked by asterisk

comparison with 12-nucleotide target RNA, the binding of a 15-nucleotide target RNA is accompanied by pivotal rotation of PAZ domain [20]. Therefore, movements of PAZ domain are essential to adapt RNA targets of variable lengths. Furthermore, a new model for RNAi mechanism suggests that strong binding during the early stage of RNAi is essential as PAZ domain will act as a handle to peel off the RNA duplex [43]. This implies the essential role of stable binding with PAZ domain in the early stages of

Table 7 Correlation analysis for RNAi activity and the measured parameters produced by the docking server

	Estimated free energy	Inhibition constant Ki	vDw + Hbond + desolvation energy	Electrostatic energy	Total intermolecular energy	Interaction surface	RL/FL
Estimated free energy	1.00						
Inhibition constant Ki	0.826*	1.00					
vDw + Hbond + desolvation energy	0.386	0.173	1.00				
Electrostatic energy	0.358	0.345	0.124	1.00			
Total intermolecular energy	0.508*	0.307	0.894*	0.457*	1.00		
Interaction surface	−0.143	−0.003	−0.385	−0.173	−0.339	1.00	
RL/FL	0.217	0.329	0.39*	0.238	−0.294	0.58*	1.00

The used template is derived from PDB ID 4EI1 (bound with guanosine). Pearson's correlation coefficient is calculated by STATA. Data showing significant correlation at 0.05 level are marked by asterisk

Table 8 Correlation analysis for RNAi activity and the measured parameters produced by the docking server

	Estimated free energy	Inhibition constant Ki	vDw + Hbond + desolvation energy	Electrostatic energy	Total intermolecular energy	Interaction surface	RL/FL
Estimated free energy	1.00						
Inhibition constant Ki	0.402*	1.00					
vDw + Hbond + desolvation energy	0.071	−0.478*	1.00				
Electrostatic energy	−0.099	−0.222	0.337	1.00			
Total intermolecular energy	0.063	−0.493*	0.962*	0.473*	1.00		
Interaction surface	0.554*	0.134	−0.238	−0.194	−0.278	1.00	
RL/FL	0.421*	0.009	0.178	0.085	−0.096	0.421*	1.00

The used template is derived from PDB ID 4F3T (bound with uridine). Pearson's correlation coefficient is calculated by STATA. Data showing significant correlation at 0.05 level are marked by asterisk

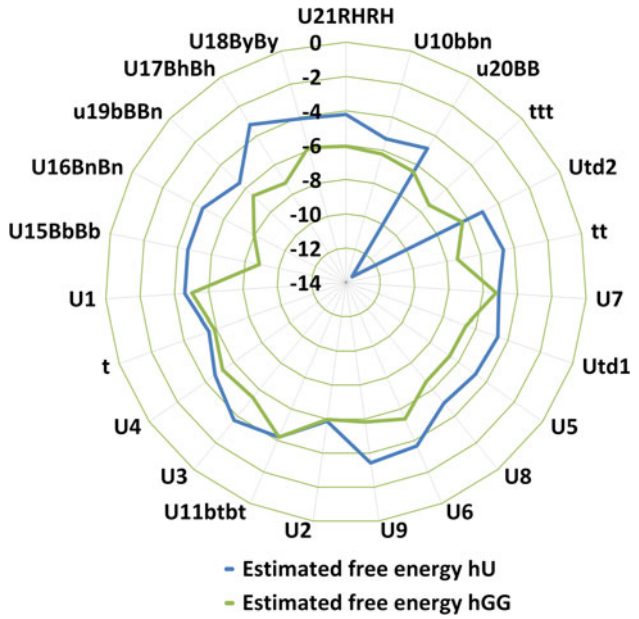

Fig. 4 Star plot of the estimated free energy calculated by the docking server. The plot is representing the estimated free energy data by using the structure of human Ago2 PAZ domain bound with uridine (hU) or guanosine (hGG). For clarity, compounds U12, U13 and U14 are removed from the plot

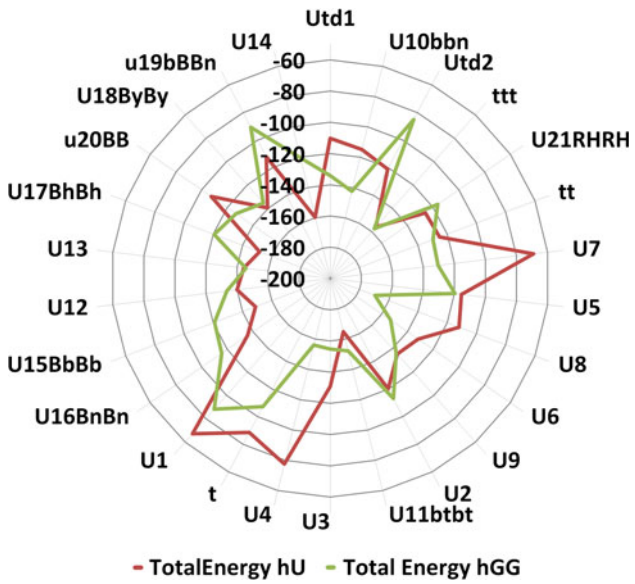

Fig. 5 Star plot of the estimated total binding energy calculated by iGEMDOCK. The plot is representing the estimated total binding energy data by using the structure of human Ago2 PAZ domain bound with uridine (hU) or guanosine (hGG)

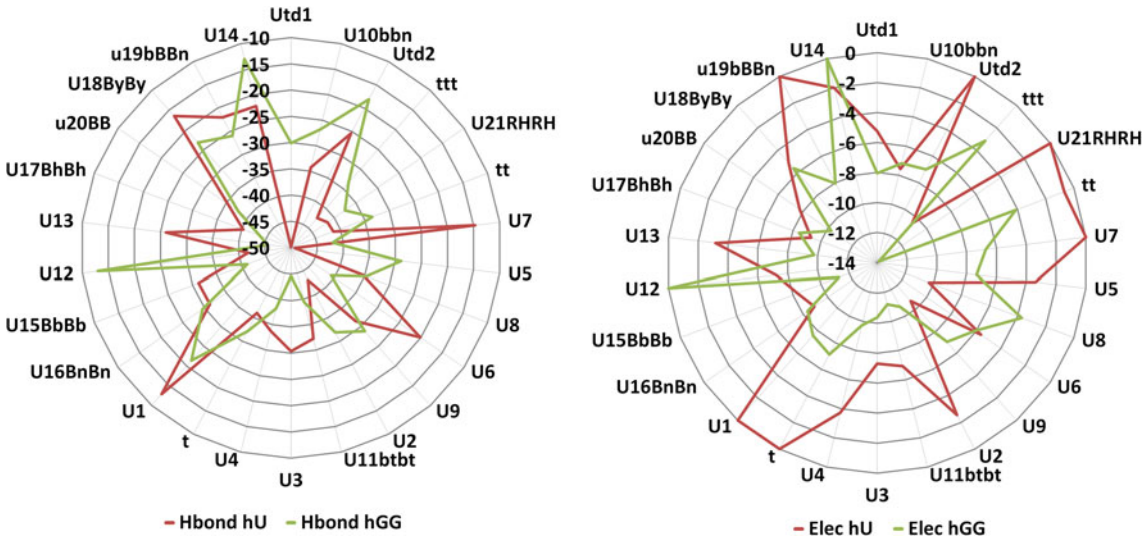

Fig. 6 Star plot of the estimated values of hydrogen bonding and electrostatic energy calculated by iGEMDOCK. The *plot* is representing the estimated values of hydrogen bonding (*left*) and electrostatic energy (*right*) by using the structure of human Ago2 PAZ domain bound with uridine (hU) or guanosine (hGG)

RNAi process. Taken together, we suggest that the stable or stronger interactions with PAZ domain will be essential for proper unwinding and release of the passenger strand and more stable binding durng the total RNAi process.

Conclusions

We examined the forces governing the recognition of siRNA by the PAZ domain and their in vivo association by using a computational approach. Previously, we provided a correlation between the measured RNAi efficacy and the calculated binding parameters by using a structural model from the *Drosophila* Ago2 PAZ domain. Further, in this short report, we provide the same correlation based on the recently resolved structures of human Ago2 PAZ domain. We identified a difference in topology of the binding site and substrate conformation. Such a difference is reflected computationally by the correlation of stronger binding affinity with higher RNAi efficacy. The size of compounds was a constantly correlated parameter, regardless the structure model used. A smaller interaction surface was correlated with higher RNAi efficacy with considerable statistical significance. Markers of strong binding as the free energy and total interaction energy were positively correlated with RNAi efficacy.

Acknowledgments Research support from Ministry of Education, Culture, Sports, Science and Technology (MEXT) and Grants-in-Aid for scientific Research (Grant No. 24390025) from the Japan Society for the Promotion of Science (JSPS).The authors provide that "The funders had no role in study design, data collection and analysis, decision to publish, or preparation of the manuscript".

References

1. Tian Y, Simanshu DK, Ma JB, Patel DJ (2011) Structural basis for piRNA 2′-*O*-methylated 3′-end recognition by Piwi PAZ (Piwi/Argonaute/Zwille) domains. Proc Natl Acad Sci USA 108(3):903–910. doi:10.1073/pnas.1017762108
2. Kim VN, Han J, Siomi MC (2009) Biogenesis of small RNAs in animals. Nat Rev Mol Cell Biol 10(2):126–139. doi:10.1038/nrm2632
3. Frank F, Sonenberg N, Nagar B (2010) Structural basis for 5′-nucleotide base-specific recognition of guide RNA by human AGO2. Nature 465(7299):818–822. doi:10.1038/nature09039
4. Yan KS, Yan S, Farooq A, Han A, Zeng L, Zhou MM (2003) Structure and conserved RNA binding of the PAZ domain. Nature 426(6965):468–474. doi:10.1038/nature02129
5. Lingel A, Simon B, Izaurralde E, Sattler M (2004) Nucleic acid 3′-end recognition by the Argonaute2 PAZ domain. Nat Struct Mol Biol 11(6):576–577. doi:10.1038/nsmb777
6. Crunkhorn S (2013) Trial watch: pioneering RNAi therapy shows antitumour activity in humans. Nat Rev Drug Discov 12(3):178. doi:10.1038/nrd3962
7. Rao DD, Wang Z, Senzer N, Nemunaitis J (2013) RNA interference and personalized cancer therapy. Discov Med 15(81):101–110
8. Singhania R, Khairuddin N, Clarke D, McMillan NA (2012) RNA interference for the treatment of papillomavirus disease. Open Virol J 6:204–215. doi:10.2174/1874357901206010204
9. Wang W, Liu C, Wang Y, Cao L (2013) Effects of the down-regulation of SnoN expression on HepG2 cell proliferation and apoptosis. Mol Med Rep 7(4):1324–1328. doi:10.3892/mmr.2013.1340
10. Wooddell CI, Rozema DB, Hossbach M, John M, Hamilton HL, Chu Q, Hegge JO, Klein JJ, Wakefield DH, Oropeza CE, Deckert J, Roehl I, Jahn-Hofmann K, Hadwiger P, Vornlocher HP, McLachlan A, Lewis DL (2013) Hepatocyte-targeted RNAi therapeutics for the treatment of chronic hepatitis B virus infection. Mol Ther. doi:10.1038/mt.2013.31
11. Li H, Zhou S, Li T, Liu Z, Wu J, Zeng G, Liu C, Gong J (2012) Suppression of BCRP expression and restoration of sensitivity to

chemotherapy in multidrug-resistant HCC Cell Line HEPG2/ADM by RNA interference. Hepatogastroenterology 59(119): 2238–2242. doi:10.5754/hge11781
12. Huang HY, Chiang BL (2009) siRNA as a therapy for asthma. Curr Opin Mol Ther 11(6):652–663
13. Seguin RM, Ferrari N (2009) Emerging oligonucleotide therapies for asthma and chronic obstructive pulmonary disease. Expert Opin Investig Drugs 18(10):1505–1517. doi:10.1517/13543780903179294
14. Presumey J, Duroux-Richard I, Courties G, Apparailly F (2010) Cationic liposome formulations for RNAi-based validation of therapeutic targets in rheumatoid arthritis. Curr Opin Mol Ther 12(3):325–330
15. Courties G, Presumey J, Duroux-Richard I, Jorgensen C, Apparailly F (2009) RNA interference-based gene therapy for successful treatment of rheumatoid arthritis. Expert Opin Biol Ther 9(5):535–538. doi:10.1517/14712590902926089
16. Li F, Mahato RI (2011) RNA interference for improving the outcome of islet transplantation. Adv Drug Deliv Rev 63(1–2):47–68. doi:10.1016/j.addr.2010.11.003
17. Kubowicz P, Zelaszczyk D, Pekala E (2013) RNAi in Clinical Studies. Curr Med Chem 20(14):1801–1816. doi:10.2174/09298673113209990118
18. Shi L, Cui S, Engel JD, Tanabe O (2013) Lysine-specific demethylase 1 is a therapeutic target for fetal hemoglobin induction. Nat Med. doi:10.1038/nm.3101
19. Kandeel M, Kitade Y (2013) Computational analysis of siRNA recognition by the Ago2 PAZ domain and identification of the determinants of RNA-induced gene silencing. PLoS ONE 8(2):e57140. doi:10.1371/journal.pone.0057140
20. Wang Y, Juranek S, Li H, Sheng G, Wardle GS, Tuschl T, Patel DJ (2009) Nucleation, propagation and cleavage of target RNAs in Ago silencing complexes. Nature 461(7265):754–761. doi:10.1038/nature08434
21. Gu S, Jin L, Huang Y, Zhang F, Kay MA (2012) Slicing-independent RISC activation requires the argonaute PAZ domain. Curr Biol 22(16):1536–1542. doi:10.1016/j.cub.2012.06.040
22. Somoza A, Terrazas M, Eritja R (2010) Modified siRNAs for the study of the PAZ domain. Chem Commun (Camb) 46(24): 4270–4272. doi:10.1039/c003221b
23. Yoshikawa K, Ogata A, Matsuda C, Kohara M, Iba H, Kitade Y, Ueno Y (2011) Incorporation of biaryl units into the 5′ and 3′ ends of sense and antisense strands of siRNA duplexes improves strand selectivity and nuclease resistance. Bioconjug Chem 22(1):42–49. doi:10.1021/bc100301w
24. Gong W, Desaulniers JP (2012) Gene-silencing properties of siRNAs that contain internal amide-bond linkages. Bioorg Med Chem Lett 22(22):6934–6937. doi:10.1016/j.bmcl.2012.09.009
25. Avino A, Ocampo SM, Perales JC, Eritja R (2012) Synthesis and in vitro inhibition properties of siRNA conjugates carrying acridine and quindoline moieties. Chem Biodivers 9(3):557–566. doi:10.1002/cbdv.201100321
26. Zeng L, Zhang Q, Yan K, Zhou MM (2011) Structural insights into piRNA recognition by the human PIWI-like 1 PAZ domain. Proteins 79(6):2004–2009. doi:10.1002/prot.23003
27. Elkayam E, Kuhn CD, Tocilj A, Haase AD, Greene EM, Hannon GJ, Joshua-Tor L (2012) The structure of human argonaute-2 in complex with miR-20a. Cell 150(1):100–110. doi:10.1016/j.cell.2012.05.017
28. Schirle NT, MacRae IJ (2012) The crystal structure of human Argonaute2. Science 336(6084):1037–1040. doi:10.1126/science.1221551
29. Taniho K, Nakashima R, Kandeel M, Kitamura Y, Kitade Y (2012) Synthesis and biological properties of chemically modified siRNAs bearing 1-deoxy-D-ribofuranose in their 3′-overhang region. Bioorg Med Chem Lett 22(7):2518–2521. doi:10.1016/j.bmcl.2012.01.132
30. Kuboe S, Yoda M, Ogata A, Kitade Y, Tomari Y, Ueno Y (2010) Diazirine-containing RNA photocrosslinking probes for the study of siRNA-protein interactions. Chem Commun (Camb) 46(39):7367–7369. doi:10.1039/c0cc02450c
31. Ueno Y, Komatsuzaki S, Takasu K, Kitamura Y, Kitade Y (2009) Synthesis and properties of oligodeoxynucleotides containing biaryl units. Nucleic Acids Symp Ser (Oxf) 53:27–28. doi:10.1093/nass/nrp014
32. Ueno Y, Watanabe Y, Shibata A, Yoshikawa K, Takano T, Kohara M, Kitade Y (2009) Synthesis of nuclease-resistant siRNAs possessing universal overhangs. Bioorg Med Chem 17(5):1974–1981. doi:10.1016/j.bmc.2009.01.033
33. Ueno Y, Inoue T, Yoshida M, Yoshikawa K, Shibata A, Kitamura Y, Kitade Y (2008) Synthesis of nuclease-resistant siRNAs possessing benzene-phosphate backbones in their 3′-overhang regions. Bioorg Med Chem Lett 18(19):5194–5196. doi:10.1016/j.bmcl.2008.08.086
34. Ueno Y, Kawada K, Shibata A, Yoshikawa K, Wataya Y, Kitade Y (2008) Synthesis and silencing properties of siRNAs possessing lipophilic groups at their 3′-termini. Nucleic Acids Symp Ser (Oxf) 52:503–504. doi:10.1093/nass/nrn255
35. Ueno Y, Kato T, Sato K, Ito Y, Yoshida M, Inoue T, Shibata A, Ebihara M, Kitade Y (2005) Synthesis and properties of nucleic acid analogues consisting of a benzene-phosphate backbone. J Org Chem 70(20):7925–7935. doi:10.1021/jo050635m
36. Hsu KC, Chen YF, Lin SR, Yang JM (2011) iGEMDOCK: a graphical environment of enhancing GEMDOCK using pharmacological interactions and post-screening analysis. BMC Bioinformatics 12(Suppl 1):S33. doi:10.1186/1471210512S1S33
37. Li Y, Frenz CM, Li Z, Chen M, Wang Y, Li F, Luo C, Sun J, Bohlin L, Yang H, Wang C (2011) Virtual and in vitro bioassay screening of phytochemical inhibitors from flavonoids and isoflavones against xanthine oxidase and cyclooxygenase-2 for gout treatment. Chem Biol Drug Des. doi:10.1111/j.17470285.2011.01248.x
38. Bikadi Z, Hazai E (2009) Application of the PM6 semi-empirical method to modeling proteins enhances docking accuracy of AutoDock. J Cheminform 1:15. doi:10.1186/17582946115
39. Morris GM, Goodsell DS, Halliday RS, Huey R, Hart WE, Belew RK, Olson AJ (1998) Automated docking using a Lamarckian genetic algorithm and an empirical binding free energy function. J Comput Chem 19(14):1639–1662. doi:10.1002/(sici)1096987x(19981115)19:14<1639:aidjcc10>3.0.co;2b
40. Song JJ, Liu J, Tolia NH, Schneiderman J, Smith SK, Martienssen RA, Hannon GJ, Joshua-Tor L (2003) The crystal structure of the Argonaute2 PAZ domain reveals an RNA binding motif in RNAi effector complexes. Nat Struct Biol 10(12): 1026–1032. doi:10.1038/nsb1016
41. Lingel A, Simon B, Izaurralde E, Sattler M (2003) Structure and nucleic-acid binding of the *Drosophila* Argonaute 2 PAZ domain. Nature 426(6965):465–469. doi:10.1038/nature02123
42. Tomari Y, Zamore PD (2005) Perspective: machines for RNAi. Genes Dev 19(5):517–529. doi:10.1101/gad.1284105
43. Lee-Fowler TM, Guntur V, Dodam J, Cohn LA, DeClue AE, Reinero CR (2012) The tyrosine kinase inhibitor masitinib blunts airway inflammation and improves associated lung mechanics in a feline model of chronic allergic asthma. Int Arch Allergy Immunol 158(4):369–374. doi:10.1159/000335122